Effect of Reynolds number and concentration on modulation of turbulence by finite size neutrally buoyant particles.

Guiquan Wang, Micheline Abbas, Éric Climent

Effect of Reynolds number and concentration on modulation of turbulence by finite size neutrally buoyant particles

Guiquan Wang[1], Micheline Abbas[2] and Eric Climent[3]

[1,3]*Institut de Mécanique des Fluides de Toulouse (IMFT) - Université de Toulouse, CNRS-INPT-UPS*
1, Allée du Professeur Camille Soula - 31400 Toulouse - FRANCE
gwang@imft.fr[1], ecliment@imft.fr[3]

[2]*Laboratoire de Génie Chimique (LGC) - Université de Toulouse, CNRS-INPT-UPS*
4, Allée Emile Monso - 31030 Toulouse - FRANCE
Micheline.Abbas@ensiacet.fr

Abstract

Direct numerical simulations of particle laden flow are carried out with the Force-Coupling Method to study the effect of finite-size neutrally buoyant particles on turbulent plane Couette flow. Two particle sizes and various concentrations (from 1 to 10%) are investigated for different Reynolds numbers above the transition to turbulence. Our results show that particle dispersion is determined by a balance between hydrodynamic wall repulsion, turbulent mixing and particle induced self-diffusion. Due to the presence of particles, close to the wall, turbulence intensity is attenuated in streamwise direction but is increased in wall-normal direction. This effect is enhanced by larger particles. The stress budget is also modified with two additional components, originating from particle rigidity (Stresslet) and particle Reynolds stress. The Stresslet contribution is stronger near the wall where the strain rate is the largest whereas maximum particle turbulent stress occurs in the core region where cross-gradient mixing is induced by turbulent flow structures. Reynolds stress budgets show no significant modulation of flow turbulence by particles. The viscous dissipation rate is the main component enhanced by particles near the transition threshold.

Keywords: turbulence modulation, particle suspensions, finite size, Force-Coupling Method, plane Couette flow(pCf)

1. Introduction

In wall-bounded flows, the turbulence length scales range from the size of the smallest eddies η (micro-scale) set by the bulk Reynolds number (Re_b) and the macro-scale set by the flow geometry. It is now well established that turbulence modulation, either augmentation or attenuation, by particles depends on the ratio between particle size d and flow micro-scale. Generally speaking, turbulence attenuation happens when d/η is small while turbulence augmentation happens with bigger d/η. As for wall-bounded flows, Gore and Crowe(1989)[1] established, in their review, qualitative relationship between the flow turbulence intensity and the ratio d/l_e (l_e being the integral length scale). A critical ratio $d/l_e = 1/10$ was found, above (resp. below) which turbulence augmentation (resp. attenuation) happens. Later, Rashidi *et al.*(1990)[2] performed experiments with wall-turbulent flows laden with polystyrene particles of two different sizes ($0.12mm$ and $1.1mm$). They found that larger particles increase the number of wall ejections, leading to higher turbulent intensities and Reynolds stress as well. However, the opposite was observed for smaller particles.

In turbulent flows close to laminar-turbulent transition, understanding turbulence modulation by particles is an important issue for transport applications, as the flow regime might switch or not from turbulent to laminar. Matas *et al.*(2003)[3] examined the effect of particle size and concentration on transition by using neutrally-buoyant particles in tube flow. They observed that either small particles at any concentration or large particles only at high concentration, increase the transition threshold, whereas large particles with moderate concentration reduce this threshold. In an attempt to understand the latter situation, particle-resolved numerical simulations of pressure-driven flows revealed that at moderate concentration, particles of finite-size (with respect to the hydraulic diameter) have a significant impact on the unsteady nature of the flow, enhancing the transverse turbulent stress components and modifying the flow rotational structures (Loisel *et al.*(2013)[4], Yu *et al.*(2013)[5] and Lashgari *et al.*(2015)[6]).

In plane Couette flow (pCf) above the transition threshold, the characteristic dimension of flow rotational structures (referred as Large-Scale Structures (LSS) by Lee and Kim(1991)[7], Tsukahara *et al.*(2006)[8]) is comparable to the Couette gap width. These structures contribute to $\sim 30\%$ of Turbulence Kinetic Energy(TKE), and they have direct impact on the mean flow velocity profile. These structures play a key role in the self-sustained turbulence process, as stated by Hamilton et al.(1995)[9], Waleffe(1997)[10] and Brandt(2014)[11]. Very small neutrally buoyant particles are expected to damp the flow turbulence by increasing viscous dissipation at the smallest flow scale. However the effect of finite-size particles on the flow response is not fully understood yet. In this context, we aim to investigate numerically the flow properties laden with finite size particles. The suspension concentrations used for this work are low to moderate.

The paper is organized as following. Particular features of the Force-Coupling Method(FCM) used to simulate the suspension flow dynamics and some validations are outlined. Then statistical quantities are presented including velocity profile, concentration distribution, turbulence intensity, stress and Reynolds stress budgets. At the end of the paper, main findings are summarized in the conclusion section.

2. Simulation method and validation

The numerical approach has been presented in [4] and [12]. The numerical simulation of particle trajectories and suspension flow field is based on the Force Coupling Method (called here FCM[13], [14]). Flow equations are dynamically coupled to Lagrangian tracking of particles. The fluid is assumed to fill the

entire simulation domain, including the volume occupied by the particles. The fluid velocity and pressure fields are solutions of the mass and momentum conservation equations. The presence of the dispersed phase in the fluid is then represented by a body force distribution written as a multipole expansion in the Navier-Stokes equations. Only the first two terms of the expansion are deployed. The first term of the expansion called the monopole represents the force that the particle exerts on the fluid (due to an external forcing or particle-to-particle contact forces). The second term, called dipole, contains the torque that a particle applies on the fluid and also ensures that the strain-rate within the fluid volume occupied by the dispersed phase is zero(particles are solid bodies). The particle translation and rotation velocities are obtained from a local weighted average of the volumetric fluid velocity (resp. rotational velocity) field over the region occupied by the particle. Particle trajectories are then obtained from numerical integration of the equation of motion.

2.1. Validation

In the absence of external forces (no gravity effect for neutrally buoyant particles), the coupling between particles and the carrier flow occurs exclusively from the force dipole forcing tensor (more specifically from the symmetric part of the dipole tensor called Stresslet) which is mainly related to the local flow strain rate. This term is calculated iteratively to ensure zero strain-rate within the fluid volume occupied by the particles. We validated the computation of the dipole tensor in the situation of a single particle located in the mid-plane of a plane Couette flow (the upper and bottom wall velocities are opposite and equal in magnitude). In this case, the particle does not experience any streamwise or wall-normal motion for symmetry reasons. Different terms of the dipole tensor were calculated and compared at steady state with previous direct numerical simulations. The method revealed to be accurate when the particle Reynolds number $Re_p < 10$ (see [4] and [12] for more details of this test).

When placed closer to one of the Couette walls, a neutrally buoyant particle has a wall-normal (or lateral) motion towards the center of the gap width at finite flow inertia (at the particle scale), as observed by Halow and Wills(1970)[15] in cylinder. DNS of 2D in pCf by J.Feng et al.(1994)[16]. Theoretical predictions were derived by Ho and Leal(1974)[17] and Vasseur and Cox(1976) [18], at quasi-steady state, in the limit of finite particle size and finite but low inertia. We tested the accuracy of the FCM in such conditions, using a Couette gap-to-particle diameter size ratio $L_y/d = 32$, and particle Reynolds number $Re_p \equiv \frac{\dot{\gamma} d^2}{4\nu} = 2.4 \times 10^{-4}$, where $\dot{\gamma}$ is the shear-rate and ν is the kinematic viscosity. Figure 1 shows the quasi-steady dimensionless wall-normal migration velocity $\frac{V_{p,y}(d/L_y)^2}{8dU_w^2/\nu}$ after 100 iterations. The simulation results are in very good agreement with the theoretical predictions obtained by Vasseur and Cox(1976) [18]. Only very close to the wall, the method is less accurate because higher orders are required in the multipole expansion to capture lubrication effect. At $Re_p = O(1)$ the equilibrium position of a particle migrating in a Poiseuille flow, due to the Segre Silberberg effect, is well captured by our method [4], [12]. However, the literature lacks quantitative information on the unsteady motion of a particle in time, at $Re_p = O(1)$. Therefore, we limit ourselves to qualitative comments on particle trajectories in the Couette gap. For the particular case shown in Fig.2, $L_y/d = 10$ and $Re_p = 1.0$, several particles (100 corresponding to volumetric concentration of 1%) are randomly seeded in the Couette gap at the beginning of the simulation. As time goes on, all particles are observed to move towards the central plane, with fluctuations in their trajectories, certainly due to pair interactions.

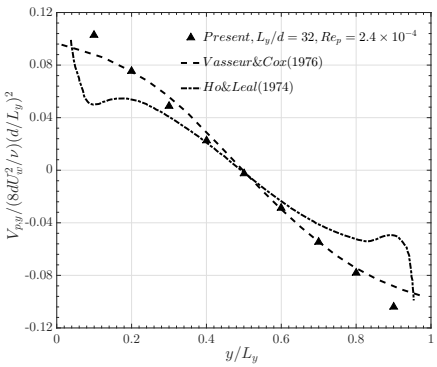

Figure 1: Validation of the numerical method: quasi-steady wall-normal velocity $\frac{V_{p,y}(d/L_y)^2}{8dU_w^2/\nu}$ of a single particle at a distance y from the wall in laminar pCf.

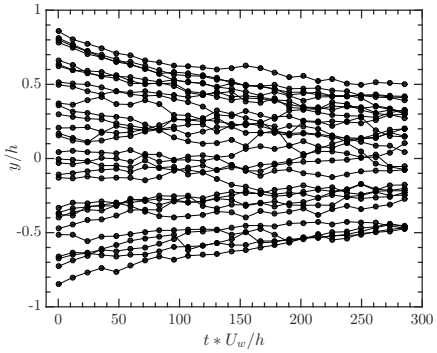

Figure 2: Trajectories of 30 (among 100) particles in Laminar pCf at $Re_p = 1$. The trajectories show particle migration towards the Couette center.

3. Flow configuration of turbulent Couette flow

The flow is sustained by two infinite planes moving in opposite directions(U_w and $-U_w$). Periodic boundary conditions are set in streamwise and spanwise directions, and no slip condition is imposed at the walls. The domain size and velocity are noted as L_x, L_y, L_z and u, v, w respectively in the flow x, wall-normal y and spanwise z directions.

The domain used for the simulations has the size of the minimal flow unit (or simply *Miniunit*) as introduced by Jiménez et al(1991) [19] and Hamilton et al.(1995) [9]. This domain allows to accommodate a single set of (periodic array of) vortical structures, which are sufficient to reproduce low-order turbulence statistics. In this domain, the turbulence is maintained when the Reynolds number is decreased down to $Re_b = \frac{U_w h}{\nu} = 340$, where the flow becomes fully laminar (h is the Couette half height). This threshold for flow relaminarization is higher than in larger pCf simulation domains ($Re_c = 324 \pm 1$,[20]) which allows longer and larger number of LSS to develop.

The grid resolution of the computational domain is set to insure 7 grid points per particle diameter. The wall units are used to scale the length and velocity such that $y^+ \equiv \frac{y u_\tau}{\nu}$, and $u^+ \equiv \frac{u}{u_\tau}$, where $u_\tau = \sqrt{\frac{\tau_w}{\rho}}$ is the friction velocity based on the wall shear stress. Table 3 contains a summary of all parameters chosen for this study.Both the bulk and frictional Reynolds numbers Re_b and Re_τ do not account for the increase value of the mixture viscosity. Due to their rigidity, particles increase the energy dissipation in the flow, leading to higher effective viscosity and therefore lower effective Reynolds number. The effective viscosity could be *a priori* estimated using models such as Eilers conclusion[21] $\nu_e = \nu[1 + \frac{1.25\Phi_v}{1-\Phi_v/0.63}]^2$, in the case of low Reynolds number and

Domain size	$L_x \times L_y \times L_z = 0.88\pi \times 1.0 \times 0.6\pi$		
Re_b	500	750	1000
Re_τ	39.5	52.2	67.3
y^+	[0-80.5]	[0-105.4]	[0-134.5]
L_y/d	10,20	20	20
$Re_p(max)$	17.5,8.75	5.83	4.38
Meshgrid	$182 \times 66 \times 128$ (for $L_y/d = 10$)		$382 \times 134 \times 256$ (for $L_y/d = 20$)
$\Phi(\%)$	[0,1,5,10]		

Table 1: Parameters of the numerical simulations. The particle Reynolds number Re_p ranges between 0 at the Couette center and $Re_p(max)$ at the wall.

homogenous suspensions. The real suspension viscosity can only be obtained by post-processing using the shear stress distribution as explained in the next section.

4. Result and discussion

4.1. Velocity profile

In turbulent single phase pCf, mean velocity profile is governed by streamwise vortices. The suspension flow profile is very close to the single phase one as seen from Fig.3, the largest discrepancy occurs for the highest concentration $\Phi = 10\%$. The velocity gradient at the wall increases with Φ, which implies higher shear stress τ_w and consequently higher energy input from the two moving walls ($\int_0^{L_x}\int_0^{L_z} U_w \tau_w(x,z)dxdz$). This behaviour is almost independent of the Reynolds number and particle size.

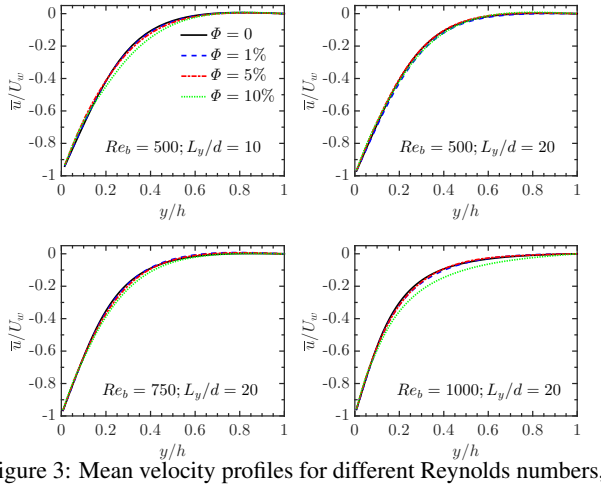

Figure 3: Mean velocity profiles for different Reynolds numbers, particle sizes and bulk concentrations. Half of the domain is shown thanks for symmetry.

4.2. Concentration spatial distribution

Fig.4 shows the mean concentration profiles for different, Re_b, particle sizes and bulk concentrations. In all cases, the concentration is higher in the Couette gap than near the walls, due to their inertial migration as explained in section 2. The profiles are relatively flat in the center due to an equilibrium reached between the inward (towards the center) inertial migration and the outward (towards the wall) shear-induced and turbulent fluxes.

A local maximum of the concentration profile appears near the wall. It is more evident at higher concentrations ($\Phi = 5\%$ and $\Phi = 10\%$) and higher Re_b. Picano *et al.*(2015)[22] noted that these peaks are of the same order of magnitude as the bulk concentration, and therefore they are not related to the turbophoretic drift typically observed in dilute suspensions when particles are heavier than the fluid. They claimed that these near-wall layers are induced by the planar symmetry of the wall and the excluded finite volume of the solid spheres. Once a particle reaches the wall the strong wall-particle lubrication interaction keeps the particle trapped close the wall. This argument could probably in average explain the local maximum. However, strong instantaneous coupling between distribution of neutrally buoyant particles and flow structures is noted in Figure 5.

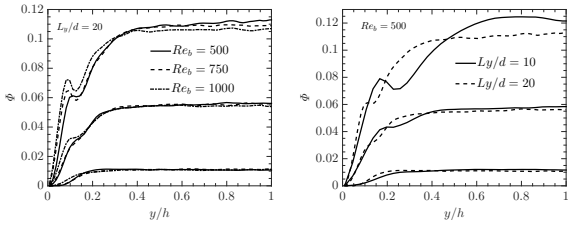

Figure 4: Mean concentration profiles for different Reynolds numbers, particle sizes and bulk concentrations. Only half of the domain is shown here. From bottom to top $\overline{\Phi}$:1%, 5%, 10%

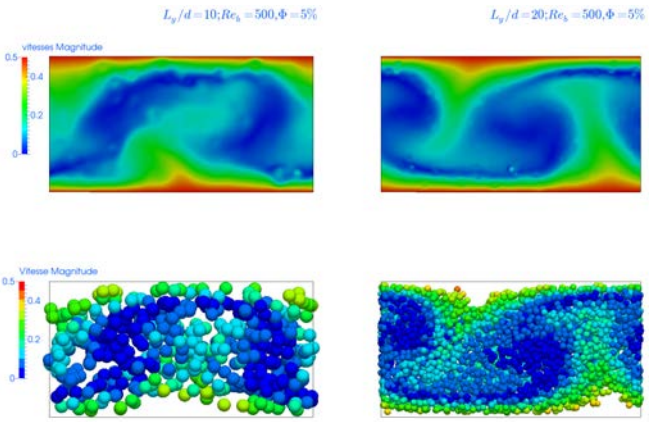

Figure 5: Upper panel: contours of the magnitude of the streamwise flow velocity in the middle cross section. Bottom panel: particle positions projected on the plane (y, z), colored according to local streamwise velocity.

4.3. Turbulence intensity

The Reynolds stress components represent all contributions to turbulent agitation. Fig.6 shows the Root-Mean-Square (R.M.S) of normal velocity fluctuations. They are scaled with u_τ which is the friction velocity of single-phase flow. Close to the Couette walls ($y^+ < 20$), u'_{rms} decreases whereas transverse components increase with concentration, especially the wall-normal direction v'_{rms}. The increase of transverse velocity fluctuations with concentration is even more pronounced with larger particles. It is not necessarily due to the increase of turbu-

lent activity. It could be related to the local concentration peak observed near the wall (at $y^+ = 8 - 10$ when $Re_b = 500$).

Also velocity fluctuations profiles in all directions are flatter in particle-laden than in single-phase flow. This indicates that particles redistribute the fluctuating energy into a more isotropic state. The trend towards isotropy is more pronounced with larger particles. Such trend is also observed in pressure-driven flow [22] with neutrally buoyant finite-size particles, whereas it is not applicable for inertial point-particles [23].

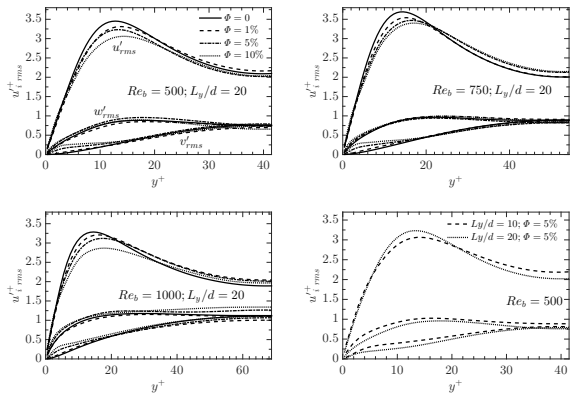

Figure 6: Turbulence intensity profiles for different Reynolds numbers, particle sizes and bulk concentrations. Only half of the domain is shown here.

4.4. *Shear stress budget*

In a Couette flow, the momentum conservation of the suspension flow in the streamwise direction leads to a constant shear stress τ_{total} across the Couette gap. In single phase flow, the shear stress is composed of two contributions, namely viscous and Reynolds stress contributions. In particle-laden flow, additional momentum transfer arises due to particle rigidity, to the forces and torques they apply on the fluid, and to their fluctuating motion with respect to local flow. The stress of a suspension flow has been derived by Batchelor(1970) [24] assuming homogeneous conditions. Batchelor introduced a decomposition of the stress into fluid and dispersed phase contributions $\Sigma_{ij} = \Sigma^{(f)}_{ij} + \Sigma^{(p)}_{ij}$ where both terms are explicitly written in eq. (1) and (2) (the dispersed phase has total surface ΣA_0 and volume ΣV_0).

$$\Sigma^{(f)}_{ij} = \underbrace{\frac{1}{V}\int_{V-\sum V_0}\left[\mu(\frac{\partial u_i}{\partial x_j}+\frac{\partial u_j}{\partial x_i})\right]dV}_{\tau_v,\text{viscous stress}} - \underbrace{\frac{1}{V}\int_{V-\sum V_0}\rho u'_i u'_j dV}_{\tau_{T_f},\text{turbulent Reynolds stress of fluid}} \quad (1)$$

$$\Sigma^{(p)}_{ij} = \underbrace{\frac{1}{V}\sum\frac{1}{2}\int_{A_0}\left[\sigma_{ik}x_j+\sigma_{jk}x_i\right]n_k dA}_{\tau_s,\text{stresslet of particle}} + \underbrace{\frac{1}{V}\sum\frac{1}{2}\int_{A_0}\left[\sigma_{ik}x_j-\sigma_{jk}x_i\right]n_k dA}_{\text{Rotlet of particle}} - \underbrace{\frac{1}{V}\int_{\sum V_0}\rho f'_i x_j dV}_{\text{stress due to external force}} - \underbrace{\frac{1}{V}\int_{\sum V_0}\rho u'_i u'_j dV}_{\tau_{T_p},\text{turbulent Reynolds stress of particle}} \quad (2)$$

In the absence of external torques and forces applied on particles, the first and last terms of eq. (2) account for the contribution of particles to the total stress. Note that the Reynolds stress components in the work of Batchelor only appear inside the particle contribution because the flow is laminar. Here, the Reynolds stress appears also in the fluid stress due to the turbulent nature of the flow. To summarize,the stress budget is:

$$\tau_{total} = \tau_v + \tau_{T_f} + \tau_s + \tau_{T_p} \quad (3)$$

similarly to what has been obtained by [22] and [25]. When scaled by the wall shear stress τ_w of each two-phase configuration, this budget becomes

$$\tau^+_{total} = 1 = \tau^+_v + \tau^+_{T_f} + \tau^+_s + \tau^+_{T_p} \quad (4)$$

Figure 7 shows the dependence on bulk concentration of all terms in eq. 4, for different Reynolds numbers and particle sizes. Our numerical simulations lead to an accurate balance for the shear stress (eq. 4). Only slight non zero budget is obtained near the wall at highest concentration ($\phi = 10\%$). Particle size has no significant effect on the stress budget components. The impact of increasing the bulk concentration on stress components depends on the wall-normal position. The fluid and particle turbulent stress components reach their maximum values in the Couette center, where cross-gradient mixing (as defined by Robinson(1990) [26]) is ensured by LSS motion [7]. When concentration increases, turbulent fluid stress is reduced whereas turbulent particle stress is augmented. Near the walls, the momentum transfer is governed by the viscous contribution. When the concentration increases, the fluid viscous stress decreases whereas the rigidity stress (stresslet) significantly increases (it becomes as high as 20% of the total stress), the latter being especially promoted by the high shear rate of the flow near the Couette walls (whereas it is almost zero in the center of the Couette gap).

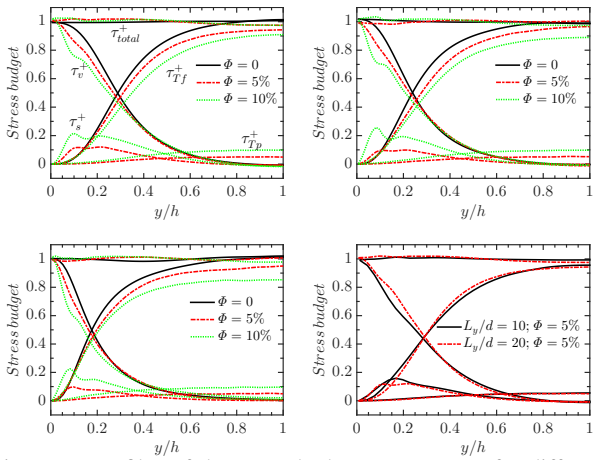

Figure 7: Profiles of the stress budget components for different Reynolds numbers, particle sizes and bulk concentrations. Only half of the domain is shown here.

4.5. *Reynolds Stress budget*

The Reynolds stress budgets describe the change rate of both Reynolds normal and shear stresses. As stated by Jeong *et al.*(1997)[27], energy is extracted from mean flow LSS to $u'u'$ due to advection. Inter-component energy transfer (from $u'u'$ to $v'v'$ and $w'w'$) occurs by vortex stretching and reorientation of vorticity from mean flow. Starting from Navier-Stokes equations coupled to particle dynamics by the Force Coupling Method, one can obtain balance equations for the velocity fluctuations or Reynolds stress (Eqn. 5) and the mean flow energy (Eqn. 6), as following:

$$\rho\left(\frac{\partial}{\partial t}\overline{u_i'u_j'}+\overline{u_k}\frac{\partial}{\partial x_k}\overline{u_i'u_j'}\right)=\overline{P'}_{ij}-\overline{\varepsilon'_{ij}}+\overline{T'_{ij}}+\overline{\Pi'_{ij}}+\overline{D'_{ij}}+\overline{FB'_{ij}} \quad (5)$$

$$\rho\left(\frac{\partial}{\partial t}(\frac{1}{2}\overline{u_i}\,\overline{u_i})+\overline{u_j}\frac{\partial}{\partial x_j}(\frac{1}{2}\overline{u_i}\,\overline{u_i})\right)=\overline{P_{ij}}-\overline{\varepsilon_{ij}}+\overline{T_{ij}}+\overline{\Pi_{ij}}+\overline{D_{ij}}+\overline{FB_{ij}} \quad (6)$$

Here the prime denotes fluctuating components. The expressions of all contributions at the right hand side of Eqns. 5 and 6 are written in table 2, and their physical meaning is the following.
P_{ij}: Production;
ε_{ij}: Dissipation;
T_{ij}: Turbulent transport;
Π_{ij}: Velocity pressure-gradient tensor decomposed into pressure rate of strain tensor Π^s_{ij} and pressure diffusion Π^d_{ij};
D_{ij}: Viscous diffusion;
FB_{ij}: Feedback from particles.

In the feedback term, the main contribution comes from the dipole forcing (stresslets) due to particle rigidity. The monopole term is different from zero only when two particles are close to contact, and its contribution to transport equations (5 and 6) is negligible in the range of concentrations used here. For this reason it is not plotted on the following figures.

Different contributions to Reynolds stress and mean flow budgets are plotted on Fig.8. In two-phase flow, the sign of all contributions is conserved with respect to the reference single phase flow case. It is observed that particles mainly increase the rate of energy dissipation of all turbulent components. Other observations can be summarized as following.

- $\overline{P'_{11}}$ is the only term to extract energy from the mean flow to produce $\overline{u'u'}$. This production term is almost unchanged by particles.
- $\overline{FB'_{22}}$ inject energy in $\overline{v'v'}$. The feedback term is maximum near the wall where the shear rate is large. It constitutes the major evident signature of the turbulent modulation by particles.
- The source term in the budget $\overline{w'w'}$, $\overline{\Pi'^s_{33}}$, is slightly stronger in two-phase flow.
- $\overline{P'_{12}}$ is the main production term of $\overline{u'v'}$ and Π'^s_{12} is the main sink term. Their respective rates are both augmented when particles are added to the flow (this figure is not drawn in this paper).

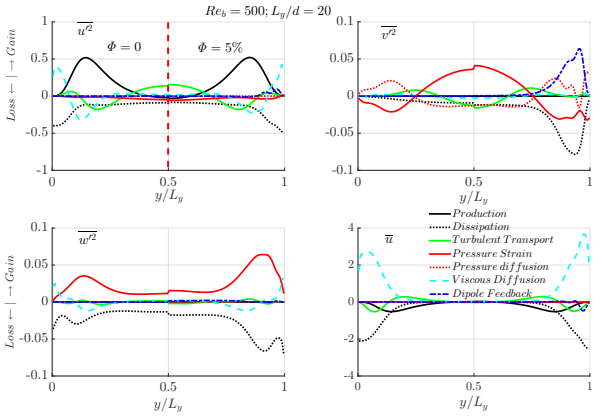

Figure 8: Comparison of contributions to the budget of $\overline{u'u'}$,$\overline{v'v'}$,$\overline{w'w'}$ and $\overline{u}\ \overline{u}$ between single phase(left part) and 5% particle-laden flows(right part), both are plotted in one figure for comparison.

5. Conclusion

The objective of our study is to evidence the interactions between particles and coherent structures of turbulent plane Couette flow. Particle-resolved numerical simulations are carried out in the case of Couette gap-to-particle diameter $L_y/d = 10$ and 20, solid volumetric concentration from 1 to 10% and Reynolds number varying from 500 to 1000.

The position of neutrally-buoyant particles in turbulent pCf results from the competition between inertial lift force, turbulent mixing and shear-induced diffusion. The concentration of particles is larger in the Couette center, with a local maximum concentration near the wall, probably due to strong ejection events pushing some particles from one wall to another where they are trapped for a while.

The partcile contribution (via the Stresslet) to the suspension flow shear stress is the strongest near the Couette wall where the strain rate is the strongest. It generates a local increase of the mixture viscosity. This effect is promoted by concentration and is independent of particle size. Reynolds shear stress induced by particles is stronger in the core region where cross-gradient mixing is ensured by LSS motion.

From the analysis of Reynolds stress budget, it is observed that particles mainly increase the rate of energy dissipation. Particles contribute to pump some energy in the wall normal direction due to the feedback term and they increase energy transfer to spanwise fluctuations by the velocity-pressure-gradient correlation. Though, they do not seem to enhance the flow turbulent nature as one may expect from the study of turbulence enhancement near the threshold of laminar-turbulent transition [3].

6. Acknowledgement

This work was granted access to the HPC resources of CALMIP under the allocation 2014-P1004 and 2015-P1004. The support provided by China Scholarship Council (CSC) from 2014 to 2017 is acknowledged. The authors would like to thank J.Feng and O. Masbernat for helpful discussions on particle migration and particle suspension dynamics, respectively, and A. Pedrono for technical support on JADIM.

References

[1] Gore, R., and Crowe, C.T., Effect of particle size on modulating turbulent intensity, *Int. J. Multiphase Flow*, vol. 15, no. 2, pp. 279–285, 1989.

[2] Rashidi, M., Hetsroni, G., and Banerjee, S., Particle-turbulence interaction in a boundary layer, *International Journal of Multiphase Flow*, vol. 16, no. 6, pp. 935 – 949, 1990.

[3] Matas, J.P., Morris, J.F., and Guazzelli, E., Transition to turbulence in particulate pipe flow, *Phys. Rev. Lett.*, vol. 90, p. 014501, 2003.

[4] Loisel, V., Abbas, M., Masbernat, O., and Climent, E., The effect of neutrally buoyant finite-size particles on channel flows in the laminar-turbulent transition regime, *Phys. Fluids*, vol. 25, no. 12, p. 123304, 2013.

[5] Yu, Z., Wu, T., Shao, X., and Lin, J., Numerical studies of the effects of large neutrally buoyant particles on the flow instability and transition to turbulence in pipe flow, *Phys. Fluids*, vol. 25, no. 4, p. 043305, 2013.

Table 2: Contributions to the Reynolds-stress transport equation (Eqn (5) and Eqn (6))

	$\overline{u}^2$	$\overline{u'u'}$	$\overline{v'v'}$	$\overline{w'w'}$	$\overline{u'v'}$
P_{ij}	$\rho\overline{u'v'}\frac{d\overline{u}}{dy}$	$-\rho\overline{u'v'}\frac{d\overline{u}}{dy}$	–	–	$-\rho\overline{v'v'}\frac{d\overline{u}}{dy}$
ε_{ij}	$-\mu(\frac{d\overline{u}}{dy})^2$	$-\mu\overline{\frac{\partial u'}{\partial x_j}\frac{\partial u'}{\partial x_j}}$	$-\mu\overline{\frac{\partial v'}{\partial x_j}\frac{\partial v'}{\partial x_j}}$	$-\mu\overline{\frac{\partial w'}{\partial x_j}\frac{\partial w'}{\partial x_j}}$	$-2\mu\overline{\frac{\partial u'}{\partial x_j}\frac{\partial v'}{\partial x_j}}$
T_{ij}	$-\rho\frac{d}{dy}(\overline{u'v'}\overline{u})$	$-\rho\frac{\partial}{\partial y}(\frac{1}{2}\overline{u'^2v'})$	$\rho\frac{\partial}{\partial y}(\frac{1}{2}\overline{v'^3})$	$\rho\frac{\partial}{\partial y}(\frac{1}{2}\overline{w'^2v'})$	$-\rho\frac{\partial}{\partial x_j}(\overline{u'v'u'_j})$
Π^s_{ij}	$\overline{p}\frac{d\overline{u}}{dx}$	$\overline{p'\frac{\partial u'}{\partial x}}$	$\overline{p'\frac{\partial v'}{\partial y}}$	$\overline{p'\frac{\partial w'}{\partial z}}$	$\overline{p'(\frac{\partial v'}{\partial x}+\frac{\partial u'}{\partial y})}$
Π^d_{ij}	$-\frac{d\overline{pu}}{dx}$	$-\overline{\frac{\partial p'u'}{\partial x}}$	$-\overline{\frac{\partial p'v'}{\partial y}}$	$-\overline{\frac{\partial p'w'}{\partial z}}$	$-\overline{(\frac{\partial p'v'}{\partial x}+\frac{\partial p'u'}{\partial y})}$
D_{ij}	$\mu\frac{d^2}{dy^2}(\frac{1}{2}\overline{u}^2)$	$\mu\frac{\partial^2}{\partial y^2}(\frac{1}{2}\overline{u'^2})$	$\mu\frac{\partial^2}{\partial y^2}(\frac{1}{2}\overline{v'^2})$	$\mu\frac{\partial^2}{\partial y^2}(\frac{1}{2}\overline{w'^2})$	$\mu\frac{\partial^2}{\partial x_j^2}(\overline{u'v'})$
FB^m_{ij}	$\overline{u}\overline{f_m(x)}$	$\overline{u'f'_m(x)}$	$\overline{v'f'_m(y)}$	$\overline{w'f'_m(z)}$	$\overline{u'f'_m(y)}+\overline{v'f'_m(x)}$
FB^d_{ij}	$\overline{u}\overline{f_d(x)}$	$\overline{u'f'_d(x)}$	$\overline{v'f'_d(y)}$	$\overline{w'f'_d(z)}$	$\overline{u'f'_d(y)}+\overline{v'f'_d(x)}$

[6] Lashgari, I., Picano, F., Breugem, W.P., and Brandt, L., Laminar, turbulent, and inertial shear-thickening regimes in channel flow of neutrally buoyant particle suspensions, *Phys. Rev. Lett.*, vol. 113, no. 25, p. 254502, 2014.

[7] Lee, M.J., and Kim, J., The structure of turbulence in a simulated plane couette flow, in *8th Symposium on Turbulent Shear Flows, Volume 1*, vol. 1, pp. 5–3, 1991.

[8] Tsukahara, T., Kawamura, H., and Shingai, K., DNS of turbulent couette flow with emphasis on the large-scale structure in the core region, *Journal of Turbulence*, no. 7, p. N19, 2006.

[9] Hamilton, J.M., Kim, J., and Waleffe, F., Regeneration mechanisms of near-wall turbulence structures, *J. Fluid Mech.*, vol. 287, pp. 317–348, 1995.

[10] Waleffe, F., On a self-sustaining process in shear flows, *Phys. Fluids*, vol. 9, no. 4, pp. 883–900, 1997.

[11] Brandt, L., The lift-up effect: The linear mechanism behind transition and turbulence in shear flows, *Eur J Mech B-Fluid*, vol. 47, pp. 80–96, 2014.

[12] Loisel, V., Abbas, M., Masbernat, O., and Climent, E., Inertia-driven particle migration and mixing in a wall-bounded laminar suspension flow, *Phys. Fluids*, vol. 27, no. 12, p. 123304, 2015.

[13] Maxey, M.R., and Patel, B., Localized force representations for particles sedimenting in stokes flow, *Int. J. Multiphase Flow*, vol. 27, no. 9, pp. 1603–1626, 2001.

[14] Lomholt, S., and Maxey, M.R., Force-coupling method for particulate two-phase flow: Stokes flow, *J. Comput. Phys.*, vol. 184, no. 2, pp. 381–405, 2003.

[15] Halow, J., and Wills, G., Radial migration of spherical particles in couette systems, *AIChE J.*, vol. 16, no. 2, pp. 281–286, 1970.

[16] Feng, J., Hu, H., and Joseph, D., Direct simulation of initial value problems for the motion of solid bodies in a newtonian fluid. part 2. couette and poiseuille flows, *J. Fluid Mech.*, vol. 277, no. 271, pp. 271–301, 1994.

[17] Ho, B., and Leal, L., Inertial migration of rigid spheres in two-dimensional unidirectional flows, *J. Fluid Mech.*, vol. 65, no. 02, pp. 365–400, 1974.

[18] Vasseur, P., and Cox, R., The lateral migration of a spherical particle in two-dimensional shear flows, *J. Fluid Mech.*, vol. 78, no. 02, pp. 385–413, 1976.

[19] Jiménez, J., and Moin, P., The minimal flow unit in near-wall turbulence, *J. Fluid Mech.*, vol. 225, pp. 213–240, 1991.

[20] Duguet, Y., Schlatter, P., and Henningson, D.S., Formation of turbulent patterns near the onset of transition in plane couette flow, *J. Fluid Mech.*, vol. 650, pp. 119–129, 2010.

[21] Stickel, J.J., and Powell, R.L., Fluid mechanics and rheology of dense suspensions, *Annu. Rev. Fluid Mech.*, vol. 37, pp. 129–149, 2005.

[22] Picano, F., Breugem, W.P., and Brandt, L., Turbulent channel flow of dense suspensions of neutrally buoyant spheres, *J. Fluid Mech.*, vol. 764, pp. 463–487, 2015.

[23] Richter, D.H., and Sullivan, P.P., Momentum transfer in a turbulent, particle-laden couette flow, *Phys. Fluids*, vol. 25, no. 5, p. 053304, 2013.

[24] Batchelor, G.K., The stress system in a suspension of force-free particles, *J. Fluid Mech.*, vol. 41, no. 03, pp. 545–570, 1970.

[25] Zhang, Q., and Prosperetti, A., Physics-based analysis of the hydrodynamic stress in a fluid-particle system, *Phys. Fluids*, vol. 22, no. 3, p. 033306, 2010.

[26] Robinson, S.K., A review of vortex structures and associated coherent motions in turbulent boundary layers, in *Structure of Turbulence and Drag Reduction*, pp. 23–50, Springer, 1990.

[27] Jeong, J., Hussain, F., Schoppa,W., and Kim, J., Coherent structures near the wall in a turbulent channel flow, *J. Fluid Mech.*, vol. 332, pp. 185–214, 1997.